

Hellenic Mediterranean University

Department of Electrical & Computer Engineering

The Stratakis Lab, Ultrafast Laser Micro and Nano Processing Laboratory

Master Thesis

«Charge energy dynamics investigation by Transient Absorption Spectroscopy on polymer composites with Single Wall Carbon Nanotubes and Ionic Liquid fillers, for thermoelectric applications. »

by

Rasouli Aggeliki

Supervisor

Dr. Stratakis Emmanuel, IESL

Dr. Konidakis Ioannis, IESL

MsC Nanotechnology for Energy Applications

Heraklion, 2023

My deepest gratitude to

Dr. Ioannis Konidakis for the guidance and the support he provided me throughout the duration of my Master's dissertation.

Dr. Emmanuel Stratakis for the inspiration and the chance to be a part of ULMNP.

Contents

Summary 3
1. Introduction 3
1.1 Thermoelectric materials 3
1.2 Motivation 12
1.3 Objectives and approach 13
2. Experimental section 14
2.1 Samples preparation 14
2.2 Experimental methods 15
3. Experimental results 20
3.1 Morphology 20
3.2 Charge extraction dynamics 21
4. Conclusions 27
Acknowledgements 28
References 28

Summary

In light of the ongoing demand for more efficient energy consumption and more sustainable energy sources, thermoelectric (TE)-based energy conversion is becoming increasingly significant. Polymer-based composites have grown in popularity in recent years, since they provide far more ecologically friendly options, they are far less expensive, easier to produce and process, and have innately low thermal conductivity. In the present work, polymer composites based on polycarbonate (PC) filled with, single-walled carbon nanotubes (SWCNTs, 0.5 wt %) and ionic liquids (ILs, 0.5 , 3.0 wt %) were studied under the implementation of transient absorption spectroscopy (TAS), in order to shed light on linking the signal of Seebeck coefficient (S) with the optical properties of the composites, under the influence of variant pump fluences. Also, scanning electron microscopy (SEM) was used, in order to study the morphology of the samples as far as their uniformity of their surface and CNT dispersion.

1. Introduction

1.1 Thermoelectric materials

The thermoelectric effect was firstly observed in the beginning of the 19th century and was described as a combination of phenomena where either a temperature difference creates an electric potential or an electric current creates a temperature difference. These phenomena are known as Seebeck, Peltier and Thomson effects.[1]

More specifically, T.J. Seebeck discovered the first thermoelectric effect in 1821. He demonstrated that heating the junction of two distinct electrical conductors might create an electromotive force. Making a connection between wires of various metals (for example, copper and iron) can demonstrate the Seebeck effect. The wires' other ends should be connected to the terminals of a galvanometer or sensitive voltmeter. When the junction between the wires is heated, the meter registers a low voltage. (Fig. 1.1.) .[1]

J. Peltier, a French watchmaker, noticed the second of the thermoelectric phenomena thirteen years after Seebeck. He discovered that passing an electric current through a thermocouple creates a minor heating or cooling effect depending on the direction of the current. Because the Peltier effect is usually accompanied by the Joule heating effect, it is difficult to show using metallic thermocouples. Sometimes the only thing that can be done is to demonstrate that there is less heating when the current is flowing in one way rather than the other.[1]

It appears that the Seebeck and Peltier phenomena were not initially recognized as interdependent. W. Thomson, on the other hand, recognized this interdependence in 1855. He was able to establish a link between the coefficients that explain the Seebeck and Peltier effects by applying thermodynamic theory to the situation. His hypothesis also demonstrated the existence of a third thermoelectric effect in a homogeneous conductor. This action, now known as the Thomson effect, consists of reversible heating or cooling when an electric current flows and a temperature gradient exists. Now it is comprehensible that electric current is conveyed via a conductor by electrons with varying energy in various materials. When a current flows from one material to another, the energy carried by electrons changes, with the difference manifesting as heating or cooling at the junction, known as the Peltier effect. Similarly, when the junction is heated, electrons can move from the material with the lowest energy to the material with the highest energy, resulting in an electromotive force. Thomson's research shown that a thermocouple is a form of heat engine that may be used as a device to generate energy from heat or as a heat pump or refrigerator. However, thermocouples are often ineffective because the reversible thermoelectric effects are invariably accompanied by the irreversible processes of Joule heating and thermal conduction.[1]

The development of semiconductor thermocouples has resulted in the development of thermoelectric generators with high enough efficiency for particular applications. Nonetheless, thermoelectric energy converters' performance has always been lower to that of the greatest conventional machines. In reality, from the development of semiconductor thermoelements until the end of the twentieth century, there was minimal advancement in thermoelectric materials. However, various new concepts for material enhancement have been proposed in recent years, and it appears that substantial progress is being achieved, at least on a laboratory scale. It is fair to anticipate that this research will soon lead to a considerably broader use of thermoelectric effects.[1]

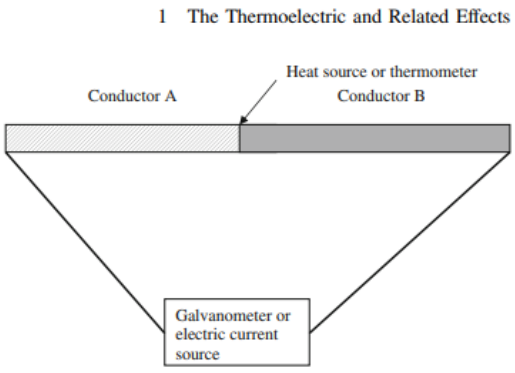


Figure. 1.1. *Experiment to demonstrate the Seebeck and Peltier effects.*[1]

For the measurement of the thermoelectric (TE) properties of a material, someone must take into account the electrical conductivity (σ), the Seebeck coefficient (S) and the power factor (PF). The performance of thermoelectric devices is directly dependent on the temperature gradient (ΔT) and an inherent material property, the thermoelectric figure of merit (ZT). The thermoelectric efficiency is determined for power production by combining the Carnot efficiency ($\Delta T/T_{hot}$) and the figure of merit ZT, as stated in eq. (1.1), where T_{hot} and T_{cold} are the temperatures of the hot and cold ends of a thermoelectric module, respectively, and ΔT is their difference. The expression $(1 + ZT_{avg})^{1/2}$ changes with the ZT_{avg} average temperature. According to this equation, increased efficiency necessitates both high ZT values and a substantial temperature differential across the thermoelectric materials. Current thermoelectric devices have a ZT of 0.8 and function at only around 5-6% efficiency. By raising ZT by a factor of four, and depending on ΔT, the estimated efficiency rises to 30%, a very appealing proposition.[2]

The difficulty in developing high ZT thermoelectric materials is attaining high electrical conductivity, high thermoelectric power and low thermal conductivity (κ) in the same solid. The dimensionless thermoelectric figure of merit ZT= $(S^2\sigma/\kappa)$T, where T is the temperature, is defined by these characteristics. These characteristics are governed by the specifics of the electronic structure and the dispersion of charge carriers (electrons or holes), and so cannot be controlled independently. Also, the amount of PF is essential for obtaining high performance, as a high PF indicates that a high voltage and current are created.[2]

$$\eta = \frac{\Delta T}{\Delta_{hot}} \frac{\sqrt{1+ZT_{avg}} - 1}{\sqrt{1+ZT_{avg}} + \frac{T_{hot}}{T_{cold}}} \quad \text{eq. (1.1)}$$

Electrical resistance is a quality that has been measured for so long that it may seem superfluous to pay much attention to it here. However, it turns out that electrical resistance measurements on thermoelectric materials provide unique challenges. Passing a known current through a piece of metal wire and monitoring the potential difference between the ends yields the electrical resistance, R. The fundamental issue in measuring the electrical resistance of the materials of interest is that thermoelectric effects are always present unless isothermal conditions are maintained. A temperature difference between the two ends causes a Seebeck voltage that augments or opposes the resistive potential. When the temperature difference is caused by an asymmetry in the experimental setup, the problem can be solved simply by reversing the current flow. However, with good thermoelectric materials, there is a

more subtle impact that can be extremely big. The Peltier effect is caused by the passage of current and results in the establishment of a temperature differential. When the current is reversed, the Peltier heating and cooling are likewise reversed, and the potential difference above the resistive value increases either way the current runs. This effect can be utilized to calculate the thermoelectric figure of merit, but when simply the electrical conductivity eq. (1.2) is of relevance, it is a source of mistake that must be avoided.[1]

$$\sigma = \frac{A}{RL} \quad \text{eq. (1.2)}$$

R = resistance (Ω)

L = length (cm)

A = Area (cm^2)

As the Seebeck coefficient eq. (1.3), is one of the simplest numbers to measure, it is frequently used instead of, say, electrical conductivity in determining whether or not a manufacturing material meets its specifications. Simply apply a known temperature differential between the ends of a sample and watch the potential difference.[1].

$$S = \frac{V}{\Delta T} \quad \text{eq. (1.3)}$$

V = thermoelectric voltage (V)

ΔT = temperature difference (K)

In recent years, it has been found useful to include power factor, which includes both the Seebeck coefficient and the electrical conductivity. The thermal conductivity (λ), is another variable included in the determination of the figure of merit. λ is less reliant on the concentration of charge carriers since it is frequently dominated by the lattice contribution. As a result, the carrier concentration that delivers the best power factor eq. (1.4) for a particular material is generally close to the figure of merit. It is obvious that when the Fermi level advances too far into a semiconductor's forbidden gap, the power factor decreases. A non-degenerate material's Seebeck coefficient varies linearly with the Fermi energy, whereas electrical conductivity varies exponentially. Even though the square of the Seebeck coefficient is used in the formulations for the power factor or figure of merit, when the decreased Fermi energy (η) is significantly less than zero, the fast change of the electrical conductivity becomes the dominant factor.[1]

$$PF = S^2\sigma \quad \text{eq. (1.4)}$$

Attempts to maximize the power factor include the creation of new classes of materials, the doping of existing materials, and the investigation of nanoscale materials. There have been a number of experimental demonstrations of increased figures of merit in nanostructures, which have been attributed in certain cases to changes in the electrical characteristics. Even if the electrical characteristics are constant, ZT can be greater than for bulk material. This advantage is related to a reduction in lattice conductivity. It is not unexpected that the dispersion of phonons becomes larger as the sample size is lowered in at least one direction.[1]

Venkatasubramanian et al. (2001) measured ZT to be 2.4 for a p-type Bi_2Te_3/Sb_2Te_3 superlattice. The electrical characteristics did alter when the superlattice period dipped below 25 nm, however this was not the primary cause for the enhanced figure of merit. The decrease in lattice conductivity was more substantial. The measurements were taken in the cross-plane direction, which was parallel to the c axis. The measured thermal conductivity was 2.2 times lower than the value in the same direction for bulk crystals. The thermal conductivity of the nanostructures is determined by Dames and Chen [12]. They pointed out that it is not just the grid conductivity that can be changed. By changing the free path length of the phonons, as well as the specific heat of the speed of sound. In principle, it is quite possible to modify the scattering. Phonon relations. However, there is a real problem if you want to make use of such modifications. For changing the specific heat, the size of the nanostructures should be smaller than the phonon wavelength. Again, the phonons remain coherent. It should be a little easier to get changes in group velocity of phonons over part of the spectrum, especially for flow perpendicular to the interface. However, due to the decrease in phonons, adding a scattering process to increase the free path length is a more profitable approach.[1]

Lin et al. [5] predicted that nanowires made of bismuth will have high Seebeck coefficients. This is supported by Heremans et al. [17] experimental work, which claims to have seen Seebeck coefficients on the order of 1 mV/K for bismuth nanowire composites. The composites were made out of wires as small as 7 nm in diameter that were formed using a vapor-phase method in porous silica and alumina templates. Electrical resistance fluctuation with temperature was found to be compatible with semiconducting rather than semi metallic behaviour. A wire with a diameter of 15 nm looked to have an energy gap of 0.18 eV, whereas a wire with a diameter of 9 nm appeared to have a gap of 0.29 or 0.39 eV. However, the fact that the 9 nm wires appeared to have a Seebeck coefficient of 105 V/K puts some doubt on the data because such a high figure is difficult to explain. The tests were difficult to execute, according to Heremans and his colleagues, since the sample resistances were in the range of 1 M-1 G, despite the fact that they were able to utilize an electrometer with an impedance of 10^{14}. Even if the measurements have to be accepted with some reservation, they do provide evidence for a

substantial energy gap in bismuth nanowires. It seems that Seebeck coefficients in excess of −200 μV/K can be reached for $Bi_{0.95}Sb_{0.005}$with an electron concentration of about 4×10^{22} per m^3 when the wire diameter is less than 30 nm. There is evidence for neutral impurity scattering of the electrons but not boundary scattering so it seems that high mobilities can still be maintained in the nanostructures.[1]

In the present work the interest gathers around thermoelectric composite materials that consist of polymer hosts and carbon nanotube (CNT) fillers, as these specific materials were examined and tested in our experimental procedure. Inorganic compounds, such as PbTe, Bi2Te3, and SnSe, are the most well-established thermoelectric materials. These materials are costly and have poor processability, brittleness, and toxicity. This circumstance necessitates further research into polymers as thermoelectric materials. Polymers are inexpensive in cost, have low heat conductivity, are highly processable and ductile, and have a low density (weight). Such polymer-based thermoelectric materials (including polymers and polymer-matrix composites) are disadvantageously low in ZT, electrical conductivity, and thermoelectric power when compared to traditional inorganic thermoelectric materials, however they present rather low thermal conductivity. As a result, research on polymer-based thermoelectric materials focuses on enhancing electrical conductivity and thermoelectric power.[3]

Other ingredients may not be required if the polymer is conductive. Polyaniline (PANI), polypyrrole (PPY), and other conductive polymers include polyacetylene (PA), polythiophene (PT), poly(3,4-ethylenedioxythiophene) (PEDOT), and poly (phenylene vinylene) (PPV) are examples of polymers. Both n-type and p-type thermoelectric materials are required for a thermoelectric energy generator. Despite the tiny output of an individual element, the series connection of alternating n-type and p-type elements results in a rather substantial electrical output. In the case of conductive polymers, the n-type and p-type behaviours are produced by doping the polymers appropriately. Doping to generate n-type conductive polymers is relatively difficult, and the resulting doped polymer is often insufficiently stable. As a result, having both n-type and p-type thermoelectric polymers, as required in a thermoelectric generator, is difficult. Furthermore, the ZT values of conductive polymers are often low, as demonstrated by a composite of conductive polymer poly(3-butylthiophene) (P3BT) and polystyrene. A polymer-polymer composite with a PEDOT matrix and PEDOT nanowires, on the other hand, has a ZT value of 0.44.

Because of the limits of conductive polymers, a frequent strategy is to combine polymers with other materials. Carbon nanotubes (CNTs) are a particularly prevalent ingredient utilized in thermoelectric polymer-matrix composites due to their electrical conductivity and the amenability for being doped. To become n-type, CNT can be doped with nitrogen or treated with polyethyleneimine (PEI). The polymer does not need to be conductive due to the conductivity of the CNTs. The electrical conductivity increases dramatically as the CNT concentration increases, but the thermal conductivity increases very marginally. The thermoelectric power is greatly boosted when a CNT forest (with aligned CNTs) is used. On the surface of the CNTs, an amino-terminated poly(3-hexylthiophene-2,5-diyl)

(P3HT) may be grafted. The grafting gives more thermoelectric power than the two parts together. CNT nanosheets sandwiched between PPY nanowires form a similar nanoscale architecture. Another nanoscale design uses polymer cores that are surrounded by CNT/polyurethane networks. Coating CNT with tiny organic compounds can also improve thermoelectric performance.[3]

Carbon nanotubes are cylindrical large molecules made up of a hexagonal arrangement of hybridized carbon atoms that can be formed by rolling up a single sheet of graphene or multiple sheets of graphene (MWCNTs) (Figure 1.2). CNTs are often capped at both ends with a hemispherical arrangement of carbon networks known as fullerenes and wrapped in a graphene sheet.[4]

Carbon nanotubes are now the subject of significant research globally. This interest in carbon nanotubes is not unexpected given their potential of exhibiting unique physical qualities that might affect a wide range of scientific and technological fields, from extremely strong composites to nanoelectronics. SWNTs can be thought of as a one-dimensional (1D) extension of various fullerene chemical clusters or as a strip cut from an infinite graphene sheet and coiled up to create a tube (Figure 1.2). Major aspects of their electrical properties may be derived using very simple Huckel-type models based on p(π) atomic orbitals. The roll-up vector $C_h = na_1 + ma_2$ = (n,m) that connects crystallographically comparable sites on a two-dimensional (2D) graphene sheet, where a_1 and a_2 are graphene lattice vectors and n and m are integers. Figure 1.3 depicts the limiting, achiral instances, (n,0) zigzag, and (n, n) armchair with dashed lines.[5]

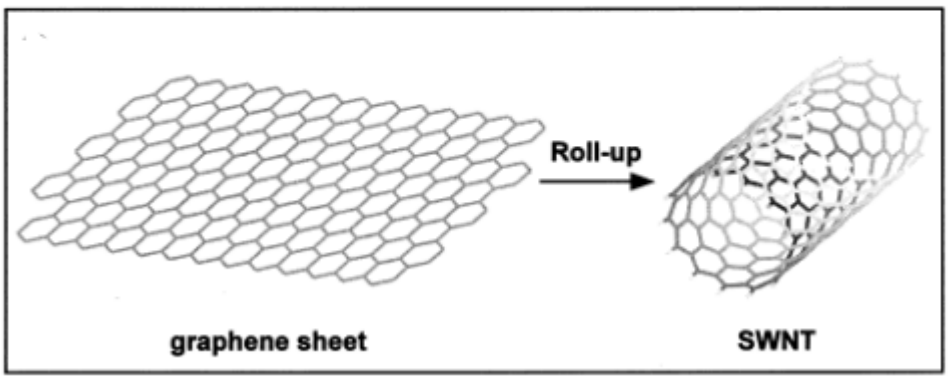


Figure. 1.2. *WNT as an extension in one-dimension (1D) of different fullerene molecular clusters or as a strip cut from an infinite graphene sheet and rolled up to form a tube*.[5]

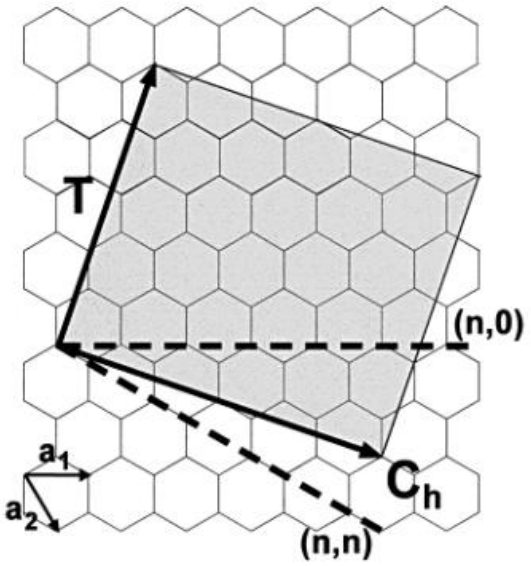


Figure. 1.3. *Schematic of a 2D graphene sheet illustrating lattice vectors a1 and a2, and the roll-up vector Ch na1 + ma2. The limiting, achiral cases of (n,0) zigzag and (n,n) armchair are indicated with dashed lines. The translation vector T is along the nanotube axis and defines the 1D unit cell. The shaded, boxed area represents the unrolled unit cell formed by T and Ch. The diagram is constructed for (n,m)) (4,2).*[5]

In our case, the tested materials were provided by InComEss program and was a pair of PC (polycarbonate)-CNTs-IL composites, which will be presented in more detail in chapter 2.1 This choice was based on previous work of Krause, et al. (2023), as the Seebeck coefficient of the chosen pair was by absolute rate almost equal. Such materials aim to a new green and cost-effective strategy for high-efficiency energy harvesting by combining new smart advanced polymer-based composite materials and structures into a single/multi-source concept to harvest electrical energy from mechanical energy and/or waste heat ambient sources, with three novel Energy Harvesting Systems (EHSs) configurations: Piezoelectric, Thermoelectric, and hybrid Thermo/PiezoElectric EHSs.

Energy harvesting is the extraction and direct conversion of energy from ambient sources into electrical energy. This method of supplying energy is also utilized when another energy source is unavailable (off-grid use) to deliver power ranging from nW to hundreds of mW to small and medium-sized electronic devices and electrical systems [1, 2]. Energy harvesting, in general, refers to an environment with consistent and well-assessed ambient energy sources. When there is a match between the available energy and the energy required, energy harvesting is used. Temperature gradient, electromagnetic radiation, light, motion, and chemical energy are examples of ambient energy sources utilized for energy harvesting. (Figure 1.4.)

The functioning of the thermoelectric generator (TEG) is critical to the collection of thermoelectric energy. According to the Seebeck effect, a TEG turns heat directly into electrical energy. The migration of charge carriers (electrons and holes) in this situation causes a temperature differential throughout this gadget. Furthermore, for various sensors and transmitters, the thermoelectric energy harvesting system may generate power ranging from hundreds of W to mW. In recent decades, experts' attention has been focused on the development of green energy technologies to reduce the usage of fossil fuels and greenhouse gas emissions. A thermoelectric harvester, generates green energy for energy harvesting, which has several advantages: maintenance-free, due to the use of a highly reliable and compact solid-state device, silent and quiet, highly efficient in terms of environmental efficiency because heat is harvested from waste heat sources and converted into electricity, operation at high maximum temperatures (up to 250°C), useful scalable applications configured to harvest large amounts of energy when needed; the ability to harvest power from both hot and cold surfaces, green energy behaviour, being environmentally friendly. Unlike thermodynamic PV systems or traditional heat engines (Rankine, Stirling), the TEG has a restricted energy conversion efficiency of 5-15%. The temperature differential throughout the TEG system, as well as the dimensionless thermoelectric figure-of-merit, have a significant influence on energy conversion efficiency. When a TEG system is in operation, the highest electric output power and efficiency are desired. Only the electric output power is relevant in waste heat recovery applications, and the heat that is not recovered is wasted. Given that thermal energy harvesting has a low efficiency (5-6%), this might be a major hurdle to its widespread use. Because of the advancement of novel thermoelectric materials, TEG efficiency has recently improved by more than 10%.[6]

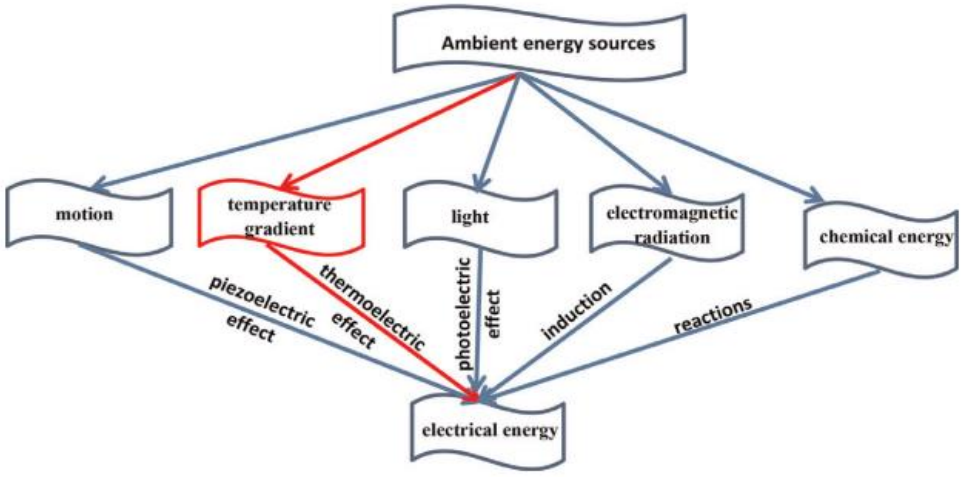


Figure. 1.4. *Energy harvesting sources.*[6]

1.2 Motivation

The measuring of a material's thermoelectric characteristics involves several unique challenges. High precision may not be required in the early phases of the development of a novel material, but once it is employed in real applications, these numbers must be understood exactly. The figure of merit, z, has a substantial influence on performance, which is influenced by three additional parameters: the square of the Seebeck coefficient, electrical conductivity, and thermal conductivity. It is critical that all three variables be tested independently, although as we will see, ZT may be determined immediately.[1]

In Beate Krause, et al. (2020) work, where the thermoelectric characteristics of nitrogen-doped MWCNTs in polypropylene-based melt-mixed nanocomposites were investigated for the first time. The results were compared to the equivalent TE characteristics of N-MWCNT buckypapers or powder packages, as well as composites comprising undoped CNTs. The TE measurements on nitrogen-doped MWCNT powders and buckypapers revealed negative Seebeck coefficients, indicating that these materials have an n-type semi-conductive characteristic. Because of the nitrogen's structure, it functions as an electron donor, transforming the CNTs' semi-conducting behaviour from a p-type hole conductor to an n-type electron conductor, as shown by a negative Seebeck value.[7]

Also, at Konidakis, et al. (2022), they melt-mixed a range of composites using single and hybrid CNT fillers based on polycarbonate (PC) and polyether ether ketone (PEEK) polymer matrices. When compared to hybrid-filler systems, the inclusion of single fillers in PC resulted in greater Seebeck coefficients and equivalent conductivities at the same loading. In contrast, hybrid-filler systems in PEEK composites can achieve better power factors than single-filler composites. Furthermore, the PC-based composites are investigated using ultrafast laser time-resolved transient absorption spectroscopy to investigate exciton lifetimes and the physical sources of free charge carrier movement inside TE films. This study's findings indicate intriguing connections between the TE parameters and the measured charge carrier dynamics. It is discovered that the Seebeck coefficient of composites is directly related to exciton lifetimes, whereas volume conductivity is independent of exciton lifetimes and is primarily determined by the average number and mobility of free charged electrons at higher energy states. Furthermore, the PC-based polymers were examined using ultrafast laser time-resolved to provide insight on the charge carrier production and transfer mechanisms inside the produced TE films. The thorough investigation of exciton dynamics, lifetime, and free charge carrier recombination yields unique insights into how the TE parameters are impacted by the CNT fillers used. In summary, the TE parameter Seebeck coefficient, is shown to be closely related to the observed charged exciton lifetimes.[8] In fact, the S-values of both PC-based single-filler and hybrid-filler composites display an approximately linear relationship on exciton lifetime (Figure 1.5. (left)), with longer exciton lifetimes

yielding higher S-values. This is explained by the fact that longerrecombination times allowing free electrons to occupy higher energy states, raising the thermovoltage potential between the hot and cold sides of the TE film.[8]

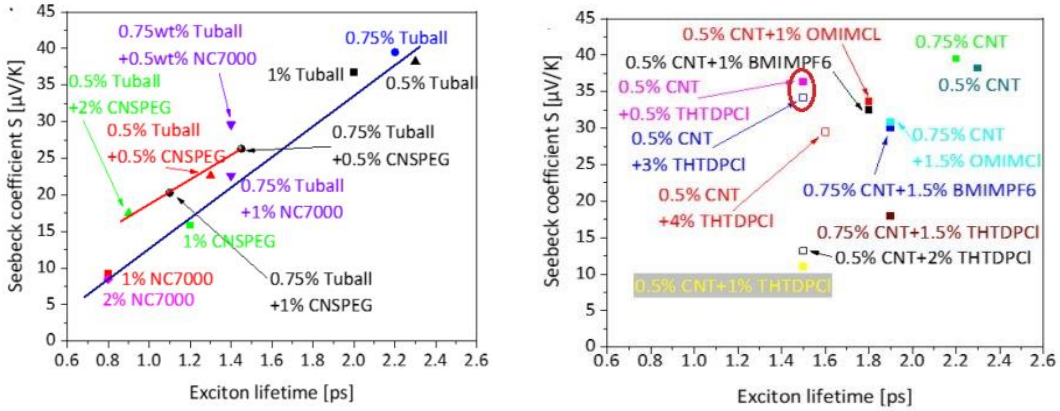


Figure. 1.5. *Seebeck coefficient vs exciton lifetimes in composites without ILs.*[9] *(left). Seebeck coefficient vs exciton lifetimes in composites without ILs, with different ILs. The empty symbols represent negative S values. Within the red circle, the samples used in our study.*[9] *(right)*

Furthermore, in the recent Beate Krause, et al. (2023) paper they studied the addition of ionic liquids (ILs) in order to transform inherently p-type single-walled CNTs (SWCNTs) into n-type melt-mixed composites based on the matrix polymers PC and PEEK, while improving the thermoelectric performance. Also, TAS was employed to clarify how the inclusion affected the conduction processes in the created PC/CNTs + IL composites, revealing formation of biexcitons when compared to the IL-free composites. Remarkably, after the addition of the IL, there was no direct correlation between S and exciton lifetimes for the IL-containing composites (Figure 1.5 (right)), while a decrease in the exciton lifetimes was observed. Also, it is noted that compounds with similar lifetimes, exhibit similar magnitude of S, but with opposite sign. Therefore, arise the need, to investigate in greater depths the sign of the Seebeck coefficient by means of TAS and try to link the sign of S with the obtained exciton lifetime.[9]In order to tackle this challenge, we employ TAS experiments in various pump fluences in order to gather more data and shed light on the correlation between the signal of S and the optical characteristics of the composites, as reflected by the time-resolved optical densities.

1.3 Objectives and approach

Our objective is to investigate the same PC/CNTs + IL composites, as presented in Beate Krause, et al. (2023) work. More specifically, the pair that was tested was PC/ 0.5 wt% Tuball + 0.5 wt% THTPD

and PC/ 0.5 wt% Tuball + 3.0 wt% THTPD. The choice of this pair was based on the fact that, both composites exhibit almost the same magnitude of Seebeck coefficient, but with opposite signs _(Table 1). This performance was caused by alterations in the IL ratio, as it was discovered that increasing the quantity of IL (THTDP) in PC/0.5 wt% SWCNT composites led to a drop in the positive Seebeck coefficient and at greater IL content, to negative S values, while the ideal content was attained at 3 wt% THTDP, because there, the S value was most negative.[9]The investigation took place at various excitation fluences with the implementation of TAS studies in order to find a correlation between the exciton dynamics and the pump fluence. Also, another goal is to manage to determine a method for receiving information, for the received negative/ positive signal of the Seebeck coefficient, through exciton lifetimes.

2. Experimental section

2.1 Samples preparation

In the present work, TAS studies were applied in PC/CNTs + IL composites. As polymer matrix polycarbonate (Makrolon 2600, Bayer MaterialScience, Germany, abbreviation PC) with a density of 1.2 g/cm3 and a melt volume-flow rate (MVR) of 12 cm3 / 10 min (300 °C/1.2 kg) was used. As an electrically conductive filler, SWCNTs of the type Tuball (carbon purity 75%, OCSiAl S.a.r.l., Luxembourg, Luxembourg, abbreviation SWCNT) were chosen for this study, and finally the selection of the IL was the trihexyltetradecylphosphonium chloride (THTDPCI; CAS 258864- 54-9, conductivity @ 25 °C 4.63 mS/cm, IoLiTec-Ionic Liquids Technologies GmbH, Germany).[9] More analytically the ratios of the samples used in TAS along with their TE properties are listed in Table.1.

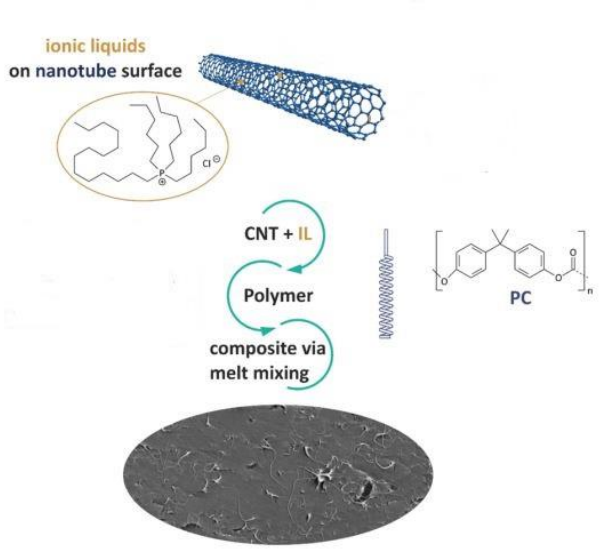


Figure. 2.1. *Chemical structure of the materials used in the study.*[9]

Table.1. *PC/CNTs + IL composites that were tested.*[9]

Sample	Vol. Conductivity (σ) [S/m]	Seebeck coefficient (S) [μV/K]	Power Factor (PF)[μW/(M·K^2)]
PC/ 0.5 wt% Tuball + 0.5 wt% THTPD	1.3	36.3 ± 0.3	1.7E-03
PC/ 0.5 wt% Tuball + 3.0 wt% THTPD	4.9	-34.2 ± 1.3	5.7E-03

2.2 Experimental methods

2.2.1 Transient Absorption Spectroscopy (TAS)

In transient absorption spectroscopy, a fraction of the molecules is promoted to an electronically excited state by means of an excitation (or pump) pulse. This fraction often ranges from 0.1% to tens of percent depending on the type of experiment. A probe pulse (that is, a pulse with such a low strength that multiphoton/multistep processes are avoided during probing) is transmitted through the sample with a delay τ relative to the pump pulse. A schematic representation of an experimental ultrafast transient absorption setup Newport (TAS-1) is shown in Figure 2.2. There the sample of interest is heated by the pump pulse in an ultrafast pump-probe experiment employing TAS, and the dynamics of the sample are monitored as a function of time at multiple wavelengths by a white-light supercontinuum probe routed with reflective optics to minimize chirp. The probing light is detected as a function of wavelength using a fibre connected multichannel detector and image spectrograph, which provides the best combination of sensitivity and dynamic range. The characteristics of the device are:

Effective spectral range: 500-1050nm.
Time window: 8000ps, **Res**.: 2nm, **Step**: 0.13fs.
Temporal resolution: 1.4*FWHM (245fs at 175fs).
Maximum spectral rate: 2kHz.
Amplifiers: Ti:Sapphire based
Repetition rates: 10 Hz to 8 kHz

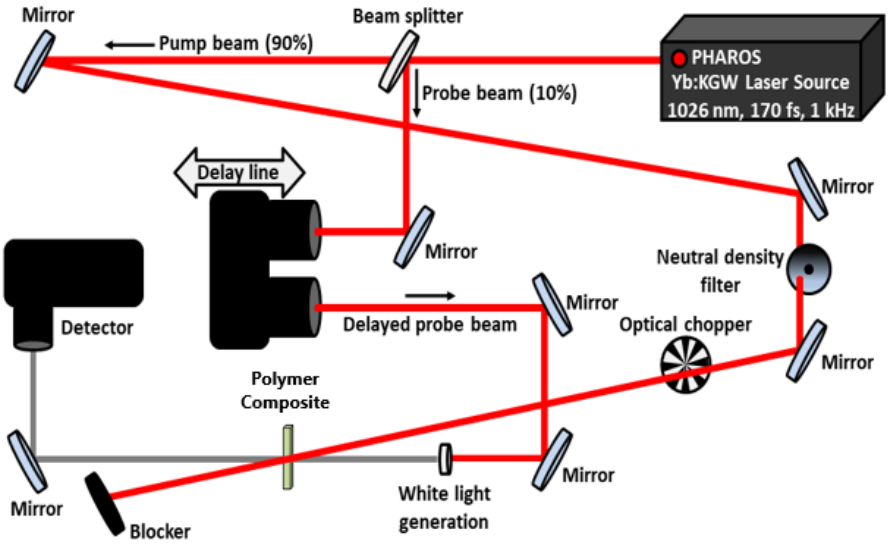


Figure 2.2 *Schematic representation of Newport (TAS-1) spectrometer.*[14]

The differential absorption spectrum, i.e., the absorption spectrum of the stimulated sample minus the absorption spectrum of the ground state, is then determined (ΔA). A ΔA profile as a function of s and wavelength λ k, i.e., a DA(λ,τ), is generated by altering the time delay τ between the pump and the probe and recording a ΔDA spectrum at each time delay. The dynamic processes that occur in the photosynthetic system under study, such as excited state energy movement, electron and/or proton transfer mechanisms, isomerization, and intersystem crossover, are described in DA(λ,τ).[10]

(1) Ground-state bleach (GSB) makes the first contribution. The number of molecules in the ground state has decreased as a fraction of the molecules have been driven to the excited state by the action of the pump pulse. As a result, the excited sample has lower ground-state absorption than the non-excited sample. Consequently, a negative signal is observed in the ΔA spectrum in the wavelength area of ground state absorption, as shown schematically in Fig. 2.3 (dashed line).

(2) The second factor is stimulated emission (SE). The Einstein coefficients for absorption from the ground to the excited state (A12) and stimulated emission from the exciting to the ground state (A21) for a two-level system are equal. When the probe pulse passes across the excited volume after the excited state has been populated, stimulated emission to the ground state will occur. Stimulated emission will occur only during optically permitted transitions and will have a spectral profile that (in general) matches the fluorescence spectrum of the excited chromophore, i.e., it is Stokes shifted with respect to the ground-state bleach. A photon from the probe pulse triggers the emission of another photon from the excited molecule, which returns to the ground state by the physical process of stimulated emission. Because the stimulated emission photon is emitted in the same direction as the probe photon, both will be

detected. The intensity of the probing pulse is so low that this operation has no discernible effect on the excited-state population. Stimulated emission causes a rise in light intensity on the detector, which corresponds to a negative ΔA signal, as shown schematically in Fig. 2.3 (dotted line). The Stokes shift in many chromophores, including bacteriochlorophyll (BChl), can be so minimal that the stimulated emission band spectrally overlaps with ground-state bleach and combines into one band.

(3) The third contribution comes from excited-state absorption. Following excitation with the pump beam, optically permitted transitions between excited (populated) states of a chromophore to higher excited states may exist in particular wavelength regions, resulting in probe pulse absorption at certain wavelengths. As a result, a positive signal is found in the DA spectrum in the wavelength area of excited-state absorption (Fig. 2.3, solid line). Again, the intensity of the probe pulse is so low that the excited-state absorption process has little effect on the excited-state population.

(4) Product absorption contributes a fourth possible contribution to the DA spectrum. After the photosynthetic, or more broadly photobiological or photochemical system, is excited, processes that result in a transitory or long-lived molecular state, such as triplet states, charge-separated states, and isomerized states, may occur. In the DA spectrum, the absorption of such a (transient) product will show as a positive signal. At wavelengths where the chromophore on which the product state dwells have ground-state absorption, a ground-state bleach will be detected.

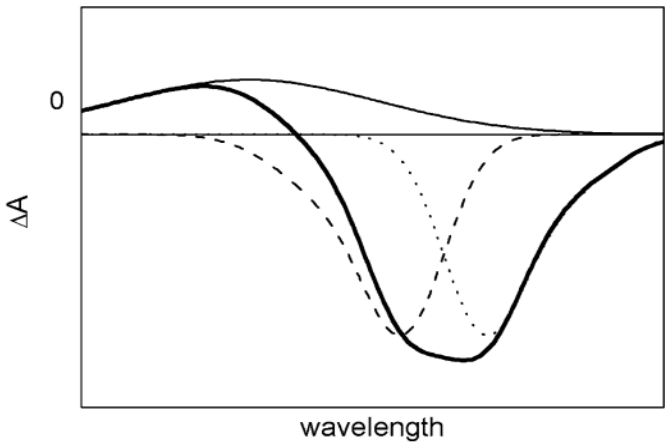


Figure 2.3. *Contributions to a DA spectrum: ground state bleach (dashed line), stimulated emission (dotted line), excited-state absorption (solid line), sum of these contributions (grey line).*[10]

The extraordinarily huge volumes of data obtained in time-resolved spectroscopic studies can be evaluated using global and target analysis approaches. A common time-resolved experiment In reality, $\Delta A(\lambda,\tau)$ is a collection of thousands of data points, i.e., tens to hundreds of wavelengths multiplied by one to two hundred data points. To extract significant information, just slice the data; for example, select one wavelength and look at its evolution over time (a so-called kinetic trace), or plot the signal at several wavelengths for a given time point (a ΔA spectrum). A common time-resolved experiment In reality, $\Delta A(\lambda,\tau)$ is a collection of thousands of data points, i.e., tens to hundreds of wavelengths multiplied by one to two hundred data points. This is typically the initial stage of data processing in which the experimentalist sees an expected (or unexpected) process.[11]

The next step in data analysis is to employ so-called global analysis techniques in an attempt to reduce the massive amount of data to a manageable number of components and spectra. The femtosecond transient absorption data are globally examined in the most basic model utilizing a kinetic model composed of progressively interconverting evolution-associated difference spectra (EADS), i.e., 1→2→3… The arrows represent sequential mono exponential decays with increasing time constants, which can be interpreted as the lifetime of each EADS. The time-zero difference spectrum is represented by the first EADS. This approach allows for a clear picture of the progression of the system's (excited) states. Based on the insights gained from this model and the raw data, a target kinetic scheme can be applied as a next stage in the research. The EADS that result from the sequential analysis are typically made up of a combination of different molecular species. In general, the EADS may well reflect molecular state mixtures. A specific kinetic model must be implemented in a target analysis technique to untangle the contributions from these chemical species and produce the spectrum signature of the "pure" excited- and product state intermediates (the so-called species-associated difference spectra, SADS). The energy and electron transport pathways can thus be evaluated in terms of a number of discrete reaction intermediates.[11]

2.2.2 Scanning Electron Microscope (SEM)

Scanning Electron Microscope uses the same operation principle as their optical counterparts. Their differences are that they use a focused beam of electrons instead of light to “image” the specimen and gain information as to its structure and composition. In SEM the electron source generates an electron beam that is propelled toward the object by employing a positive electrical potential. Using metal apertures and magnetic lenses, the electron beam is contained and focussed into a thin, focused, monochromatic beam. Electrons in the beam interact with the specimen's atoms, creating signals that carry information on its surface topography, composition, and other electrical characteristics. These interactions and effects are identified and converted into images.[12]

Electron microscopes were created in response to the limits of light microscopes, which are constrained by light physics. Electron microscopes may achieve far higher magnifications and resolving powers than light microscopes. The highest resolution of the microscope is achieved by using light sources with the smallest wavelengths. The resolution of an optical microscope is defined as the minimum distance between two spots on a specimen that can still be identified as independent entities by the observer or camera system. Resolution (r) = λ / (2NA), where λ represents the imaging wavelength and NA represents the objective numerical aperture. Magnification is the process of expanding something's appearance rather than its physical size. The ratio of image distance to object distance is defined as magnification. M = v/u, where M denotes magnification, u is object distance, and v denotes image distance. Magnification is sometimes described as the ratio of the eye's resolving power to the microscope's resolving power (δ), $M = \delta_{eye} / \delta_{microscope}$.[12]

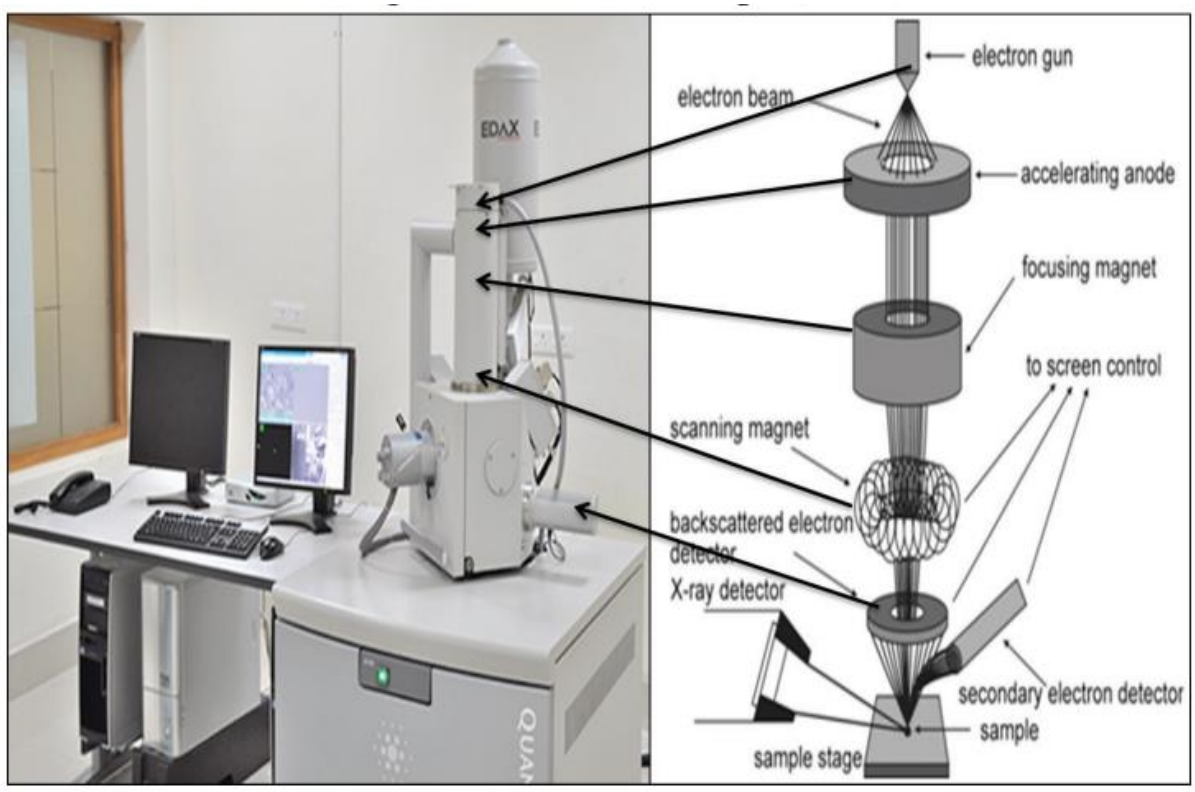


Figure 2.4. *A SEM set up.*[12]

Sputter deposition is the physical sputtering process's deposition of particles evaporated off a surface ("target"). Physical sputtering is a non-thermal vaporization process in which surface atoms are physically expelled off a solid surface due to momentum transfer from an atomic-sized energetic bombardment particle, often a gaseous ion, propelled from a plasma. Sputter deposition may be

accomplished in a vacuum by intense ion bombardment of a solid surface (sputtering target) using an ion cannon or low-pressure plasma (<5mTorr), with few or no gas phase collisions in the space between the target and the substrate. Sputter deposition is commonly used to deposit thin film metallization on semiconductor material, architectural glass coatings, and reflective coatings on compact discs (CDs), as well as magnetic films, dry film lubricants, hard coatings (tools, engine components), and ornamental coatings.[13]

3. Experimental results

3.1 Morphology

The morphological characterization of the composites was studied performing scanning electron microscopy (SEM), took place at SEM laboratory of Biology department of University of Crete. In Figure 3.1, we observe the samples after the effect of sputtering. In both composites, the lack of roughness is evident along with a continuous homogeneity across the surface. Also, the presence of ionic liquid within the composites did not show any kind of droplets, indicating the uniform dispersion of the SWCNTs within the PC based polymer matrix. Concluding all the above, it is safe to state that these kinds of compounds are very promising for TAS study at any spot of the film, because of its uniformity. Thus, considering the obtained homogeneity of the sample, it is experimentally sound to employ pump-probe spectroscopy anywhere at the surface of the composite polymer in question.

a) **b)**

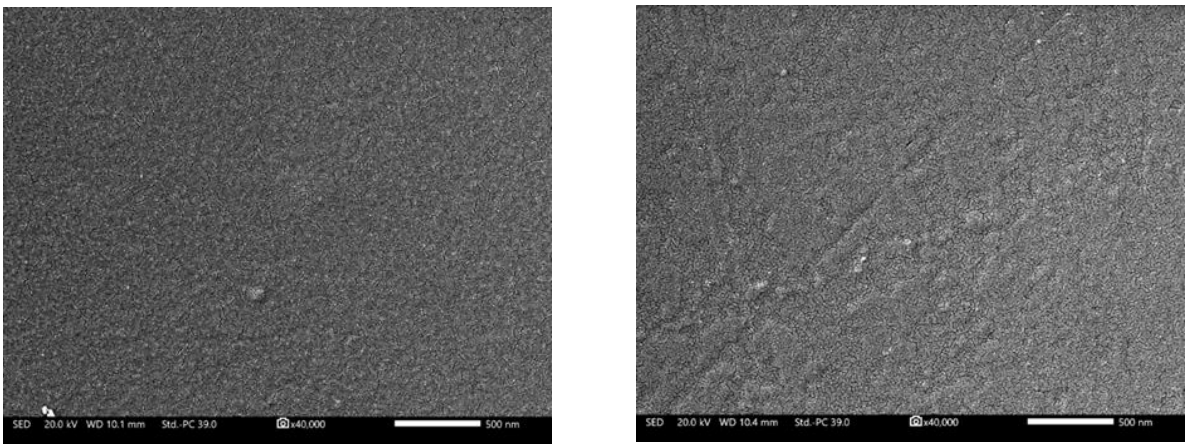


Figure 3.1 *SEM images after the sputtering of* **a)** *PC + 0.5wt% Tuball + 0.5 wt% THTPD and* **b)** *PC + 0.5 wt% Tuball + 3.0 wt% THTPD.*

3.2 Charge extraction dynamics

A typical TAS spectra (Figure 2.3) shows the optical density as a function of wavelength. Its signal indicates prevalence of photobleaching as negative ΔOD and photo absorption as positive ΔOD. The ΔOD spectrum contains contributions from three individual processes. As it was mentioned before grounds-state bleach is translated in a negative signal as a fraction of free carriers has been promoted from the ground to the excited states, so the ground-state absorption in the excited sample is less than that in the non-excited sample. Also, negative ΔOD derives from photons induced by stimulated emission, when finally, the positive contribution in ΔOD spectrum comes from the excited-state absorption.

Figure 3.2. presents the TAS spectra of the difference in optical density as a function of wavelength for various delay times, of PC 0.5 wt%_Tuball_0.5 wt % THTPD, at 10 mW, 15 mW and 20 mW pump fluence, respectively. All three spectra exhibit positive ΔOD, indicating the presence of photo absorption.

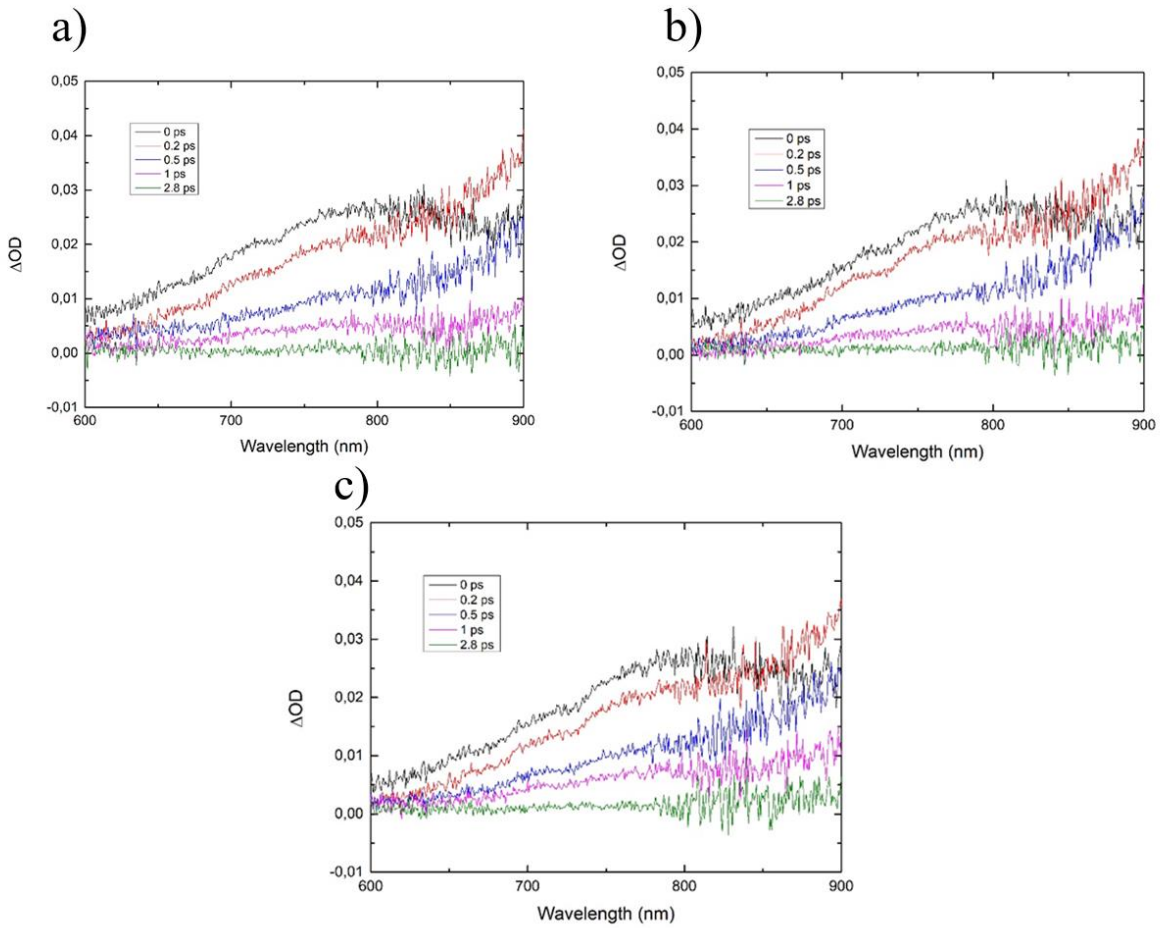


Figure 3.2 *TAS spectrum of PC 0.5 wt%_Tuball_0.5 wt % THTPD at* ***a)*** *10 mW.* ***b)*** *15 mW.* ***c)*** *20 mW.*

Moving on to the second sample, in Figure 3.3. we study the TAS spectra of PC 0.5 wt%_Tuball_3.0 wt % THTPD, at four this time different excitation fluences, 10 mW, 15 mW 20 mW and 25 mW. Again, all plots cite a positive ΔOD signal, as previously. This observation comes in accordance with the results of Krause, et al. (2023) work, where our composite PC/0.5 wt% SWCNT without the addition of ILs exhibits negative optical density upon excitation, which is a sign of photobleaching activity (Figure 3.4), when, after the incorporation of ILs, the samples exhibit positive optical densities under the same photoexcitation conditions, as in our case, where the pump fluence is varied.

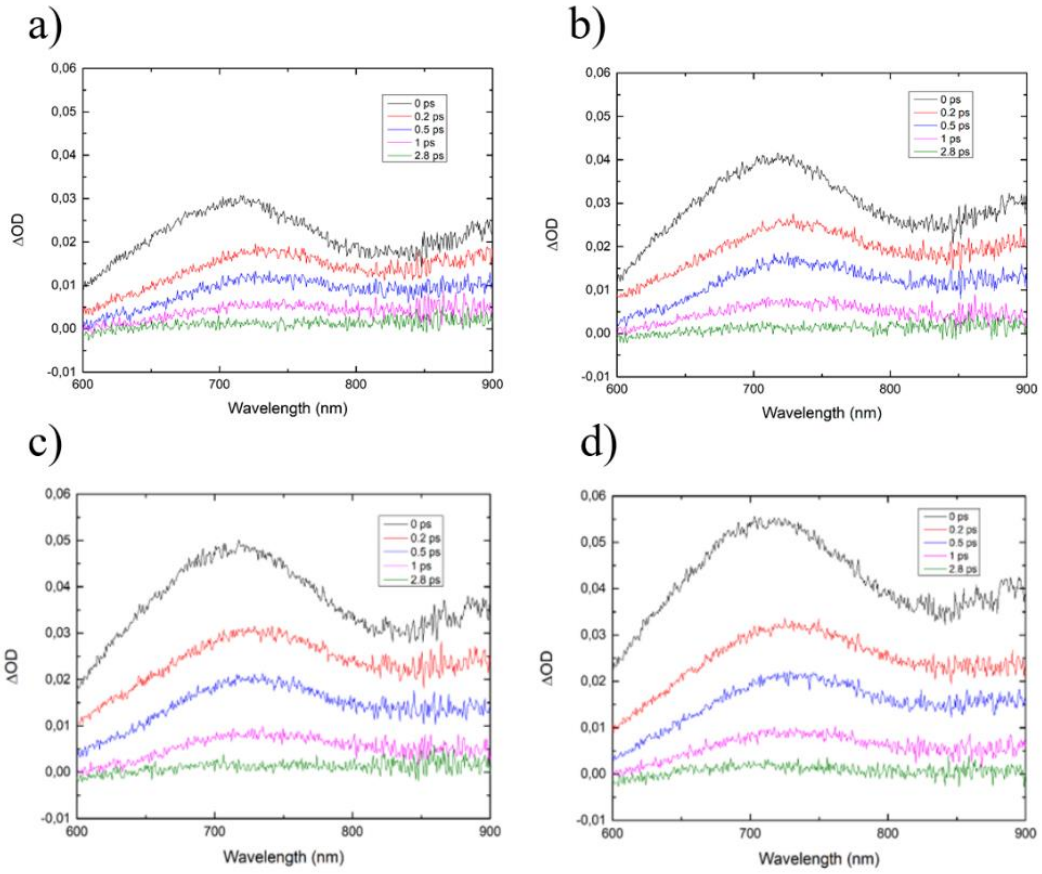


Figure 3.3. TAS spectrum of PC 0.5 wt%_Tuball_3.0 wt % THTPD at **a)** 10 mW **b)** 15 mW **c)** 20 mW **d)** 25 mW.

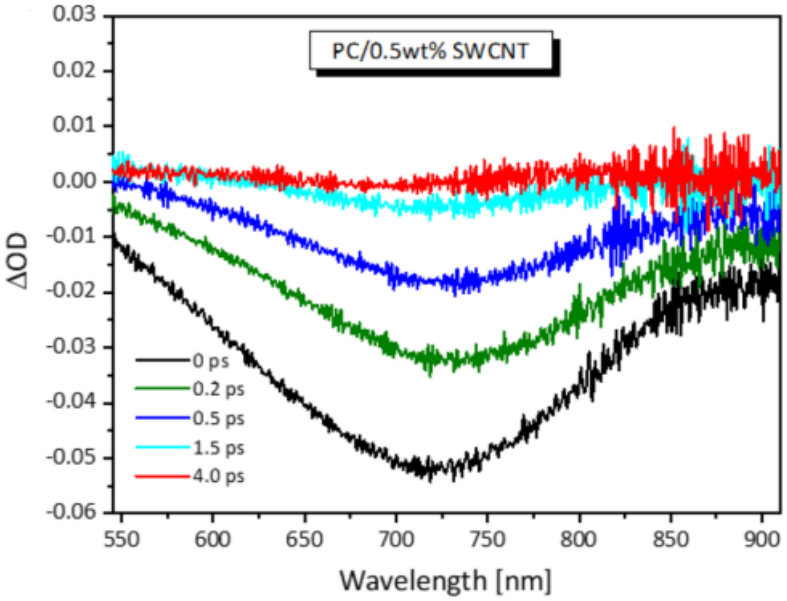


Figure 3.4 TAS spectrum of PC/0.5 wt%_SWCNTs.[9]

This phenomenon is also explained from the carrier dynamics aspect, within Krause, et al. (2023) work. Surprisingly, upon introducing the ILs within PC 0.5 wt%_Tuball_0.5 wt% THTPD and 3.0 wt% THTPD compounds, the number of excitons and excited electrons increases, promoting biexciton production to higher energy states (E11 + E22 manifold) inside the composite, as shown schematically in Figure 3.5. The latter cause the acquired PA absorption properties because fewer photoreceptors are in the ground state (GS), and hence more light is perceived (Figures 3.2 and 3.3).[9]

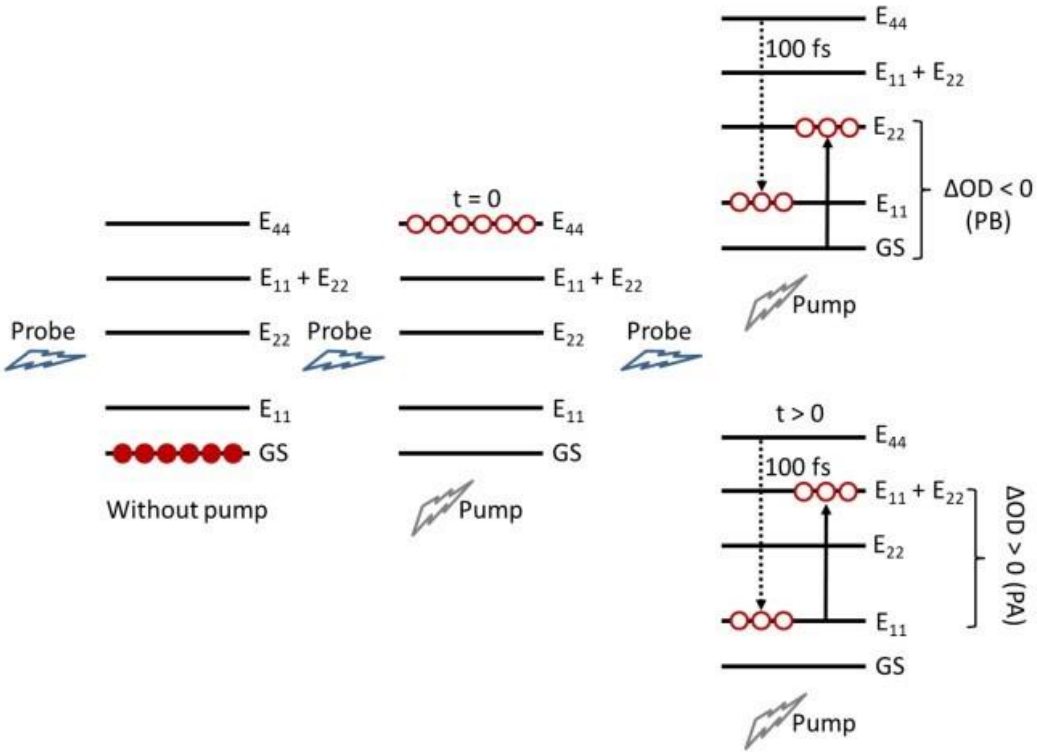


Figure 3.5. *Schematic representation of the relaxation processes throughout the pump-probe time-resolved transient absorption spectroscopy (TAS) experiment, without pump, with pump at t = 0, and with pump at t > 0.*[9]

As next step to our data analysis it is need to create exciton dynamics plot for our measurements. These plots provide us with the relaxion times of the carriers within the system, i.e., the time needed for a charged exciton to return from an excited to the ground state. Thus, we gather information about the lifetimes and the corresponding recombination processes of the free charge carriers. In order to extract a safe conclusion about our data, it is needed to compare these three curves all together, in a normalized form in the space of [0, 1] in reference to the Y axis. The key finding that derives from the study of the Figure 3.6 is that, following the increase of the pump fluence in the system leads to shorter exciton lifetimes for the PC 0.5 wt%_Tuball_0.5 wt % THTPD compound.

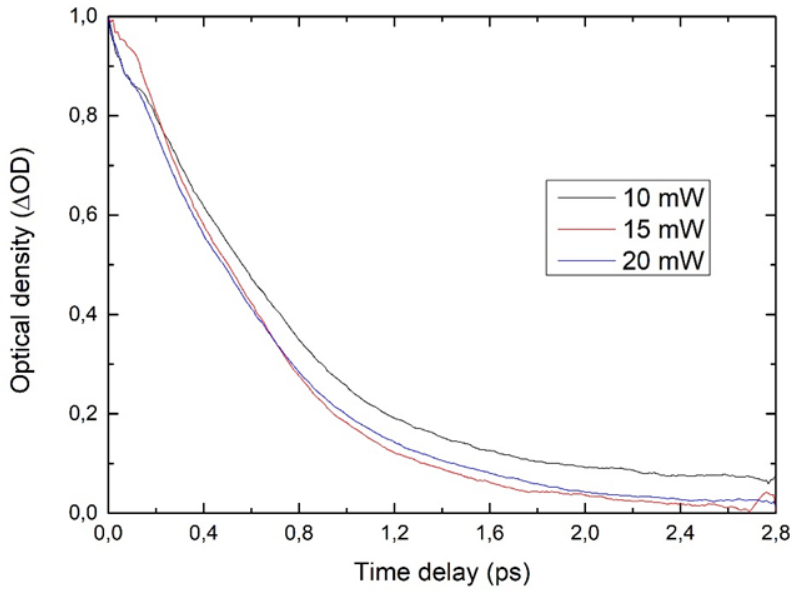


Figure 3.6 *Transient carrier dynamics for PC 0.5 wt%_Tuball_0.5 wt % THTPD, aggregated - normalized to [0,1]*

On a similar manner, Figure 3.7. presents the corresponding data for the PC 0.5 wt%_Tuball_3.0 wt % THTPD compound. By studying Figure 3.6. it is obvious that the changes in the pump fluence within the system does not bring out any difference as far as the exciton lifetimes of the carriers are concerned.

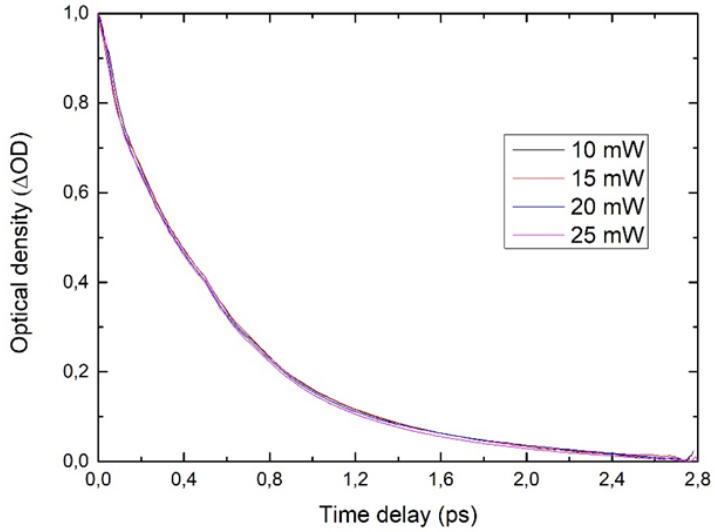


Figure 3.7 *Transient carrier dynamics for PC 0.5 wt%_Tuball_3.0 wt % THTPD, aggregated - normalized to [0,1]*

In order to have a clearer image of how the changes in the fluence, affect the exciton lifetimes, there were made plots of lifetime in dependence of pump fluence, at ΔOD at 0.3 error bar for both compounds and converted the pump fluence measurement unit from mW to $mJ\ cm^{-2}$. We have noted that the exciton lifetimes of PC 0.5 wt%_Tuball_0.5 wt % THTPD (Figure 3.8a) exhibit a clear decrease while the excitation fluence is increased i.e., exhibiting the positive S (Table.1). On the contrary, the lifetimes in PC 0.5 wt%_Tuball_3.0 wt % THTPD (Figure 3.8b) remain unaffected by the increase of the pump fluence of the system. Notably the later compound exhibits negative S (Table.1).

For the PC 0.5 wt%_Tuball_3.0 wt % THTPD, the unvarying behaviour of the carrier dynamics leads us to the conclusion, that all charge carriers populate the same band, regardless of the increase in pump fluence. On the other hand, for PC 0.5 wt%_Tuball_0.5 wt % THTPD, the decline of the exciton lifetimes, can be interpreted either, as charge carriers populating higher excitonic levels or as excitation of a larger number of carriers, that lead to faster recombination rate, with the increase of the pump. The latter is an exquisite novel finding that can help towards the understanding the signal of S, through carrier dynamics.

a) **b)**

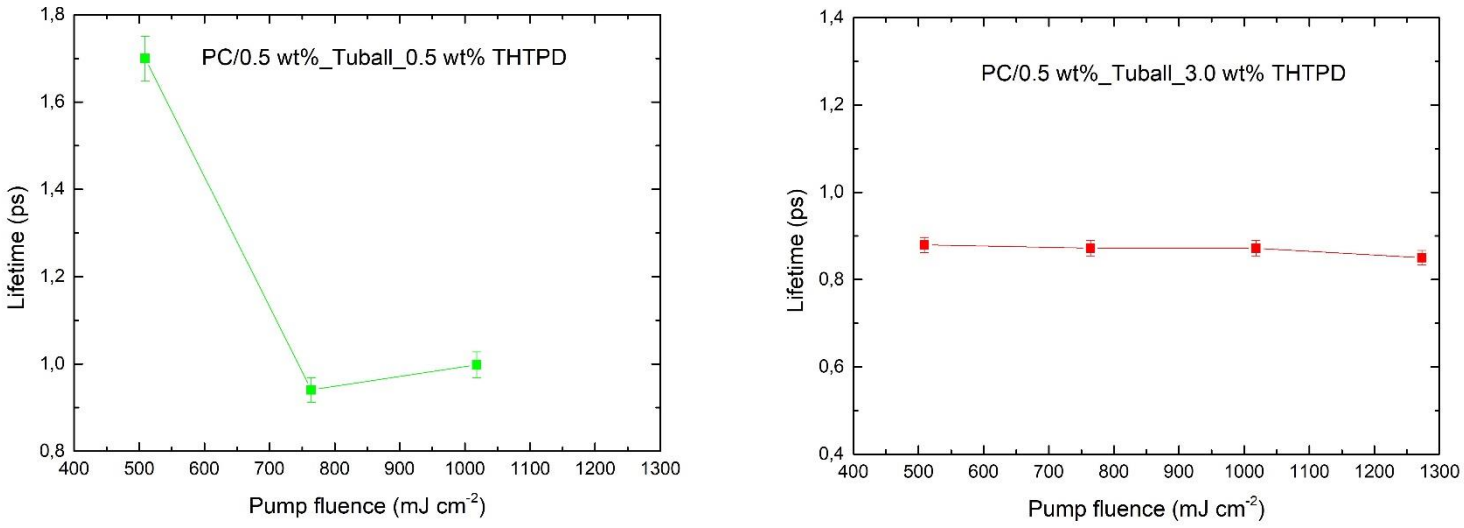


Figure 3.8. *Lifetime vs Pump fluence plot for* ***a)*** *PC 0.5 wt%_Tuball_0.5 wt % THTPD* ***b)*** *PC 0.5 wt%_Tuball_3.0 wt % THTPD.*

4. Conclusions

In conclusion, both composites exhibit equally distributed homogeneity throughout the surface and lack of surface roughness after the sputtering, while there were no droplets of any sort visible in the composites with the ionic liquid content, indicating that the SWCNTs were evenly dispersed throughout the PC-based polymer matrix. It is reasonable to say that these types of materials, due to their consistency, are particularly promising for TAS investigation at any location of the picture.

All samples exhibit positive ΔOD, indicating the presence of photo absorption, during the TAS experiments conduction. This result verifying for once more, that the addition of ILs within the polymer/SWCNTs composites, leads to shifting from photobleaching to photo absorption behavior. For the exciton lifetimes and pump fluence connection, there was concluded that the increase of pump fluence, does not influence the lifetimes of the carriers in PC 0.5 wt%_Tuball_3.0 wt % THTPD compound. On the contrary, for PC 0.5 wt%_Tuball_0.5 wt % THTPD compound, the increase in pump fluence led to shorter exciton lifetimes caused, by charge carriers which filled higher excitonic levels or by stimulation of a greater number of carriers, resulting in a quicker recombination rate as the pump power increased. This novel finding is a step closer towards the better understanding, of the relation of the decay dynamics and the pump range and the function mechanism behind sign of S, with the help of TAS. Finally, further research is demanded on the subject, including conduction of TAS experiments with more PC/CNTs + IL composite pairs, of different loadings, at various pump fluences and temperatures.

Acknowledgements

This work is funded within the frame of Horizon 2020 European Project "Innovative polymer-based composite systems for high-efficient energy scavenging and storage - InComEss," G.A. 862597.

References

[1] Goldsmid, H. Julian (2016). Introduction to Thermoelectricity. Springer Series in Materials Science. Vol. 121. Berlin, Heidelberg: Springer Berlin Heidelberg. Bibcode:2016inh..book.G. doi:10.1007/978-3-662-49256-7. ISBN 978-3-662-49255-0.

[2] Joseph R. Sootsman, Duck Young Chung, and Mercouri G. Kanatzidis (2009). New and Old Concepts in Thermoelectric Materials Angew. Chem. Int. Ed. 2009, 48, 8616 -8639.

[3] D.D.L. Chung (2018). Thermoelectric polymer-matrix structural and nonstructural composite materials, Advanced Industrial and Engineering Polymer Research 1, 61-65.

[4] Zhitomirsky, I., (2006). Electrophoretic deposition of organic inorganic nanocomposites. J. Mater. Sci. 41 (24), 81868195

[5] Teri Wang Odom, Jin-Lin Huang, Philip Kim, and Charles M. Lieber (2000). Structure and Electronic Properties of Carbon Nanotubes. J. Phys. Chem. B, 104, 2794-2809.

[6] Enescu, D. (2019). Thermoelectric Energy Harvesting: Basic Principles and Applications. Green Energy Advances. doi:10.5772/intechopen.83495

[7] Beate Krause, Ioannis Konidakis, Mohammad Arjmand , Uttandaraman Sundararaj, Robert Fuge, Marco Liebscher, Silke Hampel, Maxim Klaus, Efthymis Serpetzoglou, Emmanuel Stratakis, Petra Pötschke (2020). Nitrogen-Doped Carbon Nanotube/Polypropylene Composites with Negative Seebeck Coefficient, J. Compos. Sci., 4, 14.

[8] Ioannis Konidakis, Beate Krause, Gyu-Hyeon Park, Nithin Pulumati, Heiko Reith, Petra Pötschke, and Emmanuel Stratakis (2022). Probing the Carrier Dynamics of Polymer Composites with Single and Hybrid Carbon Nanotube Fillers for Improved Thermoelectric Performance, ACS Appl. Energy Mater., 5, 9770−9781

[9] Beate Krause, Ioannis Konidakis, Emmanuel Stratakis, Petra Pötschke (2023). Change of Conduction Mechanism in Polymer/Single Wall Carbon Nanotube Composites upon Introduction of Ionic Liquids and Their Investigation by Transient Absorption Spectroscopy: Implication for Thermoelectric Applications, ACS Appl. Nano Mater., 6, 13027−13036.

[10] R. Berera, Ri van Grondelle, John T. M. Kennis (2009). Ultrafast transient absorption spectroscopy: principles and application to photosynthetic systems, Photosynth Res., 101:105–118

[11] Van Stokkum IHM, Larsen DS, Van Grondelle R (2004). Global and target analysis of time-resolved spectra. Biochim Biophys Acta 1657:82–104

[12] K .S.Subramanian & M. Kannan Raja, K., Daya Publishing House (2018), Textbook on Fundamentals and Applications of Nanotechnology.

[13] Donald M. Mattox, William Andrew, 2nd edition (2010), Handbook of Physical Vapor Deposition (PVD) Processing, https://doi.org/10.1016/C2009-0-18800-1.

[14] Konidakis Ioannis "Laser synthesis and diagnostics of perovskite active layers"Class Lecture, Devices Processing Techniques and Characterization Methods, HMU, Heraklion 29th of March 2022